Synthesis, Experimental Testing and Multiscale Modelling of Graphene Foam/Epoxy Composite

Sajedeh Khosravani[a,b], Mohammad Homayoune Sadr[a,*], Erasmo Carrera[b], and Alfonso Pagani[b]

[a]*Department of Aerospace Engineering, Amirkabir University of Technology (Tehran Polytechnic), Tehran, Iran*
[b]*Department of Mechanical and Aerospace Engineering, Politecnico di Torino, Turin, Italy*

Abstract

Graphene foam is a three-dimensional and interconnected network of graphene. Graphene sheets, when bonded together in three dimensions, create a very lightweight porous structure with remarkable mechanical, thermal, and electrical properties. Nanocomposites made using this structure have far higher properties than conventional nanocomposites containing two-dimensional graphene sheets. In this work, randomly three-dimensional graphene foam (RGF) is synthesized from the chemical reduction of graphene oxide solution in the self-assembly method. RGF/epoxy composite is then obtained by the RTM method. Tensile test of the resulting RGF/epoxy composite samples highlight the effect of different foam preparation conditions and show a 169% and 48% increase in Young modulus and tensile strength compared to neat epoxy. Experimental results are subsequently validated using simulations based on molecular dynamics and advanced continuous micro-mechanics. In this regard, using LAMMPS, a new method is employed to obtain the initial structure of the RGF and carry out the tensile test. Also, a numerical method (CUF) based on finite element analysis of the representative unit cell is performed to obtain the mechanical properties of the RGF/epoxy composite material. The results extracted by simulations and the numerical method for composites have a good agreement with the experimental outcomings that their difference is about 1.3%.

Keywords:
Graphene foam, Mechanical properties, Molecular Dynamics, 3-D graphene modeling, CUF, Multiscale

1. INTRODUCTION

In recent years, nanotechnology has become one of the most significant areas of research in new technologies. This knowledge understands the unique properties and behavior of particles smaller than 100 nm. This knowledge pursues four main objectives by using various sciences: the synthesis of nanostructures, the study of the relationship between the properties of materials and their nanometer dimensions, the design and fabrication of nanodevices, and the creation of new structures using nanomaterials [1]. Therefore, considering the properties that nanomaterials

*Corresponding author.
Email address: sadr@aut.ac.ir (Mohammad Homayoune Sadr)

have, the use of this technology has made research in nanotechnology a scientific and industrial challenge for researchers.

Due to the exceptional properties of two-dimensional graphene, researchers have considered it in recent years, and a wide range of possibilities for the synthesis of graphene-based materials has been proposed [2]. Experimental data show that the graphene monolayer has a Young modulus of about 1000 GPa and intrinsic tensile strength of about 130 GPa, making it 100 times more potent than steel with an average density of only 2 g/cm3 [3]. Using graphene sheets and graphene-based materials in composite materials is one way to apply these properties to applications.

In the last few years, graphene sheets have been widely applied as reinforcements in polymer nanocomposites. A wide range of polymer matrices has been used for various functional materials. One of the most important of them is epoxy, which is a type of thermoset polymer [4].

In situ polymerization and solution mixing methods are used for the synthesis of most graphene /polymer composites; still, graphene or graphene oxide sheets accumulate [5] due to strong van der Waals forces, which reduce the networking. Consequently, the dispersion of the reinforcement in the polymer matrix and the expected properties are not achieved, and graphene has been challenged for use in the macro dimension. There are many methods such as surface functionalization of graphene sheets or polymer matrix chains, graphene surface modification, graphene alignment in polymer, and exfoliation of graphene sheets to improve the dispersion of graphene sheets within the matrix [6, 7]. However, none of these methods can still significantly improve the agglomeration problem, and some of these methods alter the inherent properties of graphene. On the other hand, in recent years, an efficient way of dispersing graphene sheets in the polymer matrix in the form of three-dimensional graphene hydrogel, graphene aerogel and thin-film plates [8, 9] have been introduced for this dispersion problem.

Three-dimensional graphene is an excellent way to reduce two-dimensional graphene problems. These three-dimensional graphene materials have advanced a lot due to their high performance, such as open porosity, high pore connection, large surface area, remarkable strength, etc. [10]. Graphene foam is one of the carbon foam structures that consists of several nano-shaped graphene sheets, and many pores are formed in the connection. Although graphene foam (sometimes called 3D monolayer graphene or sponge graphene) is a new material introduced in 2011 [11], its manufacturing methods vary, and research is up-to-date. In laboratory methods for synthesizing graphene hydrogels and graphene foam, the principle is to remove the force between the graphene sheets in the graphite and separate them from obtaining graphene and graphene oxide monolayers. However, for the synthesis of graphene foam, there are methods such as template directing, cross-linking method, chemical vapor deposition , and in situ reduction assembly [12]. In the following, a brief history of graphene foam reinforced composites is presented.

Li et al. [13] used the polymer vacuum injection technique in graphene foam to produce highly conductive composites for practical applications such as electronic devices, sensors, actuators, and electromagnetic shields. Bong et al. [14] used graphene foams as a filter to separate liquids such as water, oil, and so on. This measure is necessary to prevent possible environmental pollution and malfunctions of equipment or facilities in the oil industry. Ni et al. [15] produced graphene foam-reinforced polymer-based composites using resin molding and transfer. In their method, the most significant challenge is the dispersion of graphene sheets in the composite. The process of synthesizing graphene is through self-assembly. The diffusion of graphene sheets in epoxy has increased mechanical properties and the very high thermal stability of the composite. Zhao et al. [16] the effect of carbon fiber on the mechanical and thermal properties of graphene foam/polymer composites with a meager volume fraction of carbon fiber achieved good

properties, which was illustrated using scanning electron microscope (SEM) images. Zhang et al. [17] investigated the thermal behavior of a polymer composite filled with graphene foam using the finite element method. Due to the interconnected structure of graphene foam, which forms effective thermal pathways, the polymer composite reinforced with graphene foam has superior thermal properties. Chen et al. [18] in the assembly of graphene foam showed how to produce solid porous materials lighter than air. They showed that these solid materials could use for applications such as helium replacement to fill an incapacitated balloon in critical situations. Pedrielli et al. [19] performed computational research using molecular dynamics with reactive potentials and normal function on the mechanical properties and thermal conductivity of graphene foams/carbon nanotube. Their study obtained graphene foams using simulations same as a topology experimentally by growing graphene on nickel nanoparticles. Rahmani et al. [20] a model of graphene foam using simulated polycrystalline copper is presented in Molecular Dynamics software, which is used as a membrane to separate gases.
In the present study, due to the unique structure of graphene foam and its exceptional properties, the RGF is synthesized and added to epoxy as a reinforcer. The term random used in graphene foam in this work is due to creating a completely random network, both experimentally and numerically. Distributing random graphene sheets in numerical graphene foam brings it closer to laboratory methods and produces more reliable results. RGF is prepared by hydrothermal method combined with the chemical reduction of graphene oxide solution and self-assembly method called HCS in this study. The synthesis method of RGF in this work, compared to other methods, requires relatively inexpensive equipment, low process temperature, low energy consumption, and full compatibility with the environment. The resin transfer molding (RTM) method was used to fill the porous structure of RGF with epoxy. This work expects the agglomeration phenomenon to be minimized by creating RGF, and the necessary tests have been performed to show this issue. A novel molecular dynamics method is used to simulate RGF, in which the mechanical properties of RGF are numerically studied using a tensile test to confirm experiments. Finally, micro-mechanics simulations based on Carrera unified formulation (CUF) finite elements and mechanics of structure genome (MSG) are employed to obtain the mechanical properties of the RGF/epoxy composite.

2. SYNTHESIS METHODOLOGY

2.1. Materials

Graphene oxide powder 99% with 3.4-7 nanometers is provided by US Research Nanomaterials, Inc. Ammonia solution 35%, Hydroxide acid (HI) 57%, Acros, deionized water (DI) and Acetone were purchased from Swiss-composite.ch. The goal is to convert graphene oxide to graphene hydrogel using reducers such as hydroxide acid, paraffin diamine, ethylenediamine, and ascorbic acid. Epoxy Araldite LY 5052 and Aradur 5052 in a weight ratio of 100 to 38 respectively were prepared from HUNTSMAN chemical company and used in this work.

2.2. Preparation of Graphene Foam

In this work, macroscopic RGF is obtained using graphene oxide solution and a relatively simple and cost-effective synthesis method, namely the hydrothermal method, which is combined with the chemical reduction method of graphene oxide solution and the self-assembly method (HCS). The purchased graphene oxide is in graphene oxide layers, which are black in color and

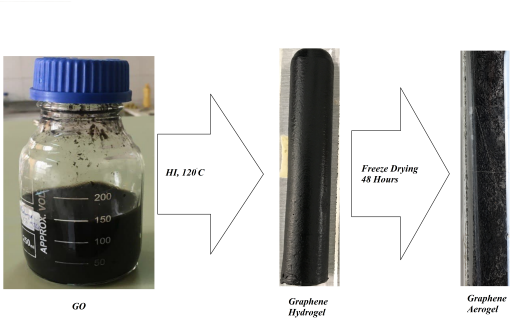

Figure 1: Preparation of solution graphene oxide, graphene hydrogel, and graphene aerogel.

powder form. The following steps have been taken to convert graphene oxide to graphene hydrogel and then graphene aerogel, the so-called RGF. First, 99% graphene oxide is mixed with DI for 10 minutes, then it is placed in an ultrasonic bath and centrifuged at 2000 rpm for 1 hour. In the next step, a reducing agent of 1.2 in graphene oxide is added to the solution. The solution is placed in an autoclave for 5 hours at a temperature of 120°C and under a certain pressure to provide carbon atoms bonding conditions in the solution. The graphene hydrogel obtained in DI is washed to remove all impurities. The resulting solution is stored in 14% ammonia for 24 hours at room temperature. After this step, as shown in Fig. 1, the three-dimensionally prepared graphene is hydrogel graphene containing a large amount of water. It is placed in a freeze dryer for 48 hours at a specific temperature and pressure to dry the graphene hydrogel. Temperature and pressure in the drying stage have a significant effect on the final product. Finally, three types of samples of RGF with different drying percentages are obtained, which are 100% dried, 95% and 85% dried RGF, respectively. In the first type, graphene hydrogel was placed in a freeze dryer at -55°C and 0.1 Torr for 48 h. Next, a vacuum furnace at a pressure of 0.06 MPa was employed for one hour to minimize sample bubbles. The second type, it is placed in the freeze dryer at -70°C and 0.075 Torr for 24 hours to dry. The vacuum is applied at a pressure of 0.07 MPa for 30 minutes. In the last type of RGF, graphene hydrogel was placed in the freeze dryer at -45°C and 0.1 torr pressure for 24 hours. It must be mentioned, in this work, four samples of each type of RGF are synthesis.

2.3. Fabrication of Epoxy Composites Reinforced by RGF

The matrix consists of two parts: Araldite LY 5052, a low viscosity epoxy resin, and Aradur 5052, a mixture of polyamines. Information for Araldite LY 5052: aspect (visual) clear liquid, viscosity at 25°C (ISO 12058-1) 1000 – 1500 MPa, density at 25°C (ISO 1675) 1.17 g/cm^3, epoxide index (ISO 3001) 6.65 – 6.85 Eq/kg, and about Aradur 5052: aspect (visual) clear liquid, viscosity at 25°C (ISO 12058-1) 40 – 60 MPa, density at 25°C (ISO 1675) 0.94 g/cm^3, Amine value (ISO 9702) 9.55 – 9.75 Eq/kg. Araldite and Aradur are combined in a weight ratio of 100 to 38.

In this work, the RTM method is used to fabricate the composite. The resin and epoxy are mixed with the percentage of weights mentioned and placed in an ultrasonic bath for 10 minutes to obliterate the epoxy bubbles. Next, the temperature of the solution is increased to 70°C, with a

stirring time is 5 minutes. The synthesized RGF is inserted into the mold and injected with the prepared epoxy into the mold. The samples are placed in a vacuum furnace pressure of 0.06 MPa in two stages for 5 minutes to remove the bubbles and then hardened at room temperature for 24 hours. The size of the mold is according to the ASTM D638 standard [21].

3. NUMERICAL MODEL

3.1. Full Atomic Models of the RGF

In this work, the structure of RGF and its mechanical properties by the Large-scale Atomic-Molecular Massively Parallel Simulator Molecular Dynamics (LAMMPS MD) package [22] are evaluated. Here a three-dimensional porous structure is obtained by the fusion graphene sheets around a metal template at high temperature that is in agreement with the works of Quin [18], Rahmani [20] and experimental in this study. A four-step method has been used to generate the structure of RGF.

In the first step, a metal polycrystalline structure is used for the formation pattern of RGF. A random polycrystalline box with dimensions of $100 \times 100 \times 100$ Å^3 consisting of 150 grains of FFC Au (lattice size=4.065 Å) is created using Atomsk software [23]. In the second step, the polycrystalline structure is divided into different grains, and some grains are removed randomly. It should be noted that the final foam density can be controlled by removing the desired number of polycrystalline grains, changing the size of the polycrystals and the size of the graphene sheets. Developing a Python code, a random number is selected that removes 135 grains from the 150 grains in the polycrystalline box. In the third step, the one-layer graphene sheet made with graphene edge type in armchair and length along x and y equal to 0.5 nm is distributed among the polycrystalline grains according to the final foam density. Fig. 2(a) shows a schematic of the graphene/Au template structure before the graphene sheet connection. In the fourth step, a carbon-carbon interaction force is used by developing a LAMMPS MD code for connection between graphene sheets. The LAMMPS MD code for the generation of RGF in detail is as follows:

1000 single-layer graphene, each layer has 24 carbon atoms and a band length of 1.42 Å, randomly distributed among the Au polycrystalline grains. Carbon atoms less than 7.5 Å away from Au atoms are removed from the simulation box. At the start of the simulation, the system pressure increases from 1 atm to 1000 atm at a temperature of 300 K by adjusting the Nose-Hoover barostat and the isothermal-isobaric (NPT) ensemble. At the second step, applying the canonical (NVT) ensemble for stabilizes at the pressure of 1000 atm and increasing the temperature from 300 K to 3000 K by setting Nose-Hoover thermostat. In the third step, NVT is used to keep the volume and temperature constant at 3,000 K. In the fourth step, the system's temperature under the same ensemble decreased to 300 K. In the last step, the system's temperature with the same ensemble balanced at 300 K. The graphene flake is compressed from the gas state to the solid-state by repeating this 5-step cycle. Each simulation step is performed for 50 ps with a time step of 0.25 ps. In this simulation, there are physical bonds between the Au atoms and the graphene sheets. It should be noted that the adaptive intermolecular reactive empirical bond order (AIREBO) [24] potential describes all interactions between carbon atoms in graphene, and boundary conditions are considered periodic in 3 directions.

By using Lennard-Jones (L-J) parameters for carbon-carbon and Au-Au atoms can be calculated these parameters for carbon-Au atoms with the formula Lorentz-Berthelot mixing role [25]:

$$\sigma_{ij} = (\sigma_{ii} + \sigma_{jj})/2 \tag{1}$$

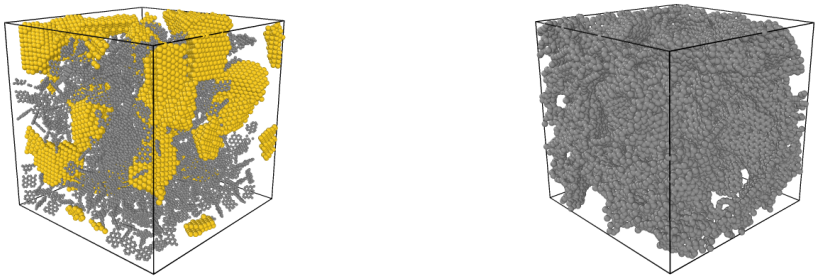

(a) (b)

Figure 2: (a) Schematic of the graphene/Au template structure before graphene sheets connection, (b) Final foam after remove Au grains .

$$\varepsilon_{ij} = \sqrt{\varepsilon_{ii} \times \varepsilon_{jj}} \tag{2}$$

Where in Eq. (1), Eq. (2) σ_{ii} and ε_{ii} are the L-J parameters of carbons atoms [20], σ_{jj} and ε_{jj} are the L-J parameters for Au atoms [26], and σ_{ij} and ε_{ij} are L-J parameters obtained between Au and carbon atoms, which are equal to 3.023 Å and 0.0316 eV, respectively. Fig. 2(b) shows that in the simulation box, after forming all the bonds and going through the heating/cooling cycles, the Au atoms are removed, and the final foam is obtained. The number of carbon-carbon bonds and the system density are measured at the end of each heating and cooling cycle.
The topology of RGF in this study is close to growing RGF on metal polycrystals in the laboratory and is different from the method presented in the reference [19].

3.2. Numerical Model of RGF/Epoxy Composite Based on CUF-UC Micromechanical Model

In order to validate the experimental analysis, a high-efficient micromechanical model based on CUF finite elements is used. This micromechanics model acts as an efficient tool for calculating the effective stiffness matrix of other properties of periodic heterogeneous composite structures.
CUF has been developed for beams, plates, and shells. Although 1D models are used in the present research as they have been demonstrated to provide the same accuracy as conventional solid elements with reduced computational efforts, see [27, 28]. Accordingly, the main direction of the micro-scale constituents (e.g., the fiber direction in the case of fiber-reinforced polymers or inclusions) is discretized employing one-dimensional finite elements whereas the cross-section is hierarchically enriched with a set of Legendre-based polynomials with non-local capabilities. In addition, the implementation of a non-isoparametric mapping technique permits the representation of the exact geometry of the constituents with no additional costs [29].
According to CUF, the 3D displacement field of the continuum can be expressed as follows:

$$\mathbf{u} = N_i(y) F_\tau(x, z) \mathbf{u}_{\tau i} \tag{3}$$

Where N_i is the 1D shape functions, F_τ is arbitrary cross-sectional polynomials which characterize the model kinematics, and $u_{\tau i}$ is the generalized unknowns. Repeated indexes denote

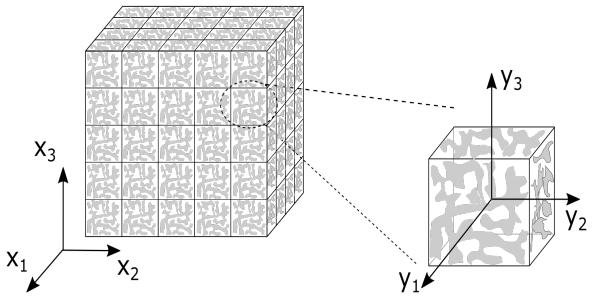

Figure 3: Coordinate reference systems of a periodic heterogeneous material and its RUC.

summation [30]. CUF-based refined beam theories are employed here to model the repeating unit cell (RUC) of RGF/epoxy composite and the MSG [31] for deriving the governing equations. MSG exploits the variational asymptotic method (VAM) to solve mechanical problems that involve smaller parameters and has been successfully applied to provide efficient solutions for composite problems, see [32, 33]. VAM can be used to carry out an asymptotic analysis of the RUC problem and obtain the effective properties and the local solutions of periodically heterogeneous materials [34] with great accuracy and efficiency. Interested readers can refer to [30] for more information. For representative purposes, Fig. 3 shows the RUC of the RGF/epoxy composite under consideration with 8.1% volume fraction of graphene in RGF and periodic boundary conditions.

In MSG, solving the stationary value problem by minimizing the difference between the strain energies of the heterogeneous structure and the equivalent homogeneous materials is expressed as follows:

$$\Pi = \frac{1}{2}\int_V C_{ijkl}\varepsilon_{ij}\varepsilon_{kl}dV - \frac{1}{2}C^*_{ijkl}\bar{\varepsilon}_{ij}\bar{\varepsilon}_{kl} \tag{4}$$

where the first expression of the system energy Π is related to the strain energy of the heterogeneous structure, indicated by the RUC, and the second is related to the homogeneous material. C_{ijkl} is a fourth-order elastic tensor and ε_{ij} is a second-order strain tensor, both of which refer to global solutions [27].

4. RESULTS AND DISCUSSION

4.1. Characterization Methods and Morphology

The synthesized RGF has a black color, porous structure, and 0.84 g/cm^3 density. Raman spectroscopy and SEM techniques are used to determine the characteristics of synthesized RGF. Graphene oxide and RGF were analyzed by Raman spectroscopy to determine the chemical properties. Raman spectroscopy with specifications (Teksam/model: Tekram) and YAG (CW) laser with a wavelength of 532 *nm* were used in all experiments. The range of spectroscopy in Raman shift is 530 to 700 and from 0 to 4400 in cm^{-1}.

Raman spectroscopy was applied to evaluate the transform from graphene oxide to RGF. Fig. 4 shows that a strong peak (G-band) and a weak peak (D-band) occur in the Raman spectra. The Raman G band is activated in sp2 carbon hybridization of the base material and indicates in-plane vibration mode. The D band is activated when defects in the Raman scattering resonance

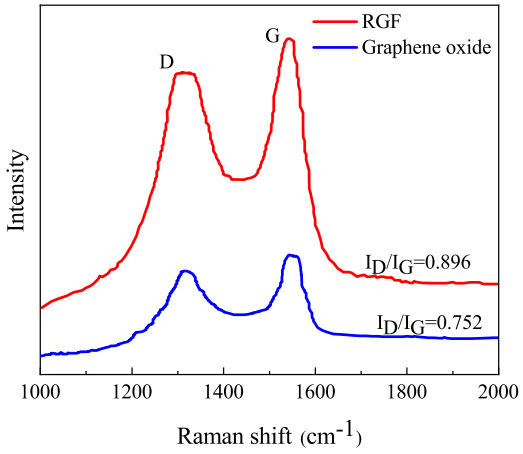

Figure 4: Raman spectroscopy of graphene oxide and RGF.

occur near the K point in the Brillouin region and show sp3-hybridized carbon. Therefore, the peak intensity ratio from D to G, which is often used to estimate the sp2 domain size of carbon, i.e., $I_D \backslash I_G$, increases from 0.752 to 0.896 after converting graphene oxide to RGF. This ratio shows the primary oxygen-containing groups removed from the graphene oxide sheets and the sp2 regenerated carbon structure. In addition, the increase in the G-band peak indicates the reconstruction of a hexagonal lattice of carbon atoms.

Also, the morphology of RGF was observed by the scanning electron microscope (MIRA TESCON). Fig. 5 shows a piece of RGF with SEM images at various magnifications of 200 μm, 20 μm, 1 μm, and 500 nm, respectively. RGFs have a three-dimensional porous network with interconnected pores. From SEM images, RGF has pore sizes in the range of 500 nm to 20 μm in diameter can be seen. The porous structure with many wrinkles is observed with different magnifications, indicating the formation of a three-dimensional RGF structure through the accumulation and binding of reduced graphene oxide sheets. The magnification image shows that graphene has an entirely rough surface. SEM images and Raman spectroscopy approve the formation of RGF.

4.2. Characterization of the Numerical Morphology

There are criteria for validating the structure of simulated RGF, which can be used to ensure the simulated form, such as experimental methods. Based on these criteria for generating RGF, the heating/cooling cycle is repeated in five-times. Each cycle increased the system temperature from 300 K to 3000 K in 250 ps and equilibrated at 300 K. Repetition of heating and cooling cycles allows a condensed structure to be generated. At the end of each cycle, the radial distribution function (RDF) diagram, density, and the number of C-C bands are measured. The density of RGF converges to 0.813 g/cm^3 at the end of the heating and cooling cycles, which is approximately equal to the density of the experimental samples in this study.

RDF diagram at the end of three first cycles plus the pre-cooling and heating cycle is shown in Fig. 6(a). RDF diagram shows that the first peak occurred at 1.42 Å, i.e., the carbon-carbon

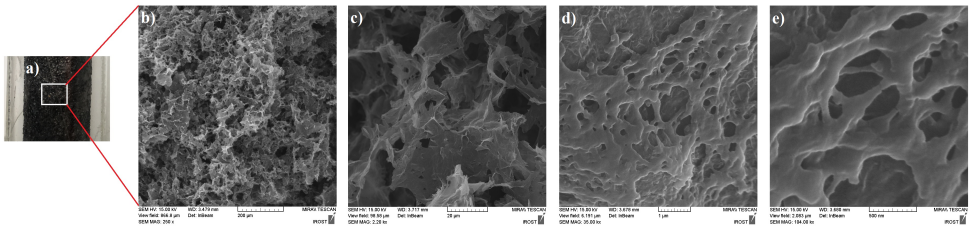

Figure 5: a) A piece of synthesized RGF and SEM images at magnification: b) 200 μm, c) 20 μm, d) 1 μm, e) 500 nm.

bond length in graphene sheets. This peak intensity increases with each heating and cooling. This increase in bonds per cycle can also be seen in the C-C bond diagram. Fig. 6(b) shows the actual number of C-C bonds in each heating/cooling cycle. In the first step, which is before the heating and cooling of the system, the total number of C-C bonds is equal to 21390. After the first heating and cooling cycle, this number reaches 23249 bonds, and similarly, in the second and third cycles, this number increase 23357 and then 23462. After the third heating/cooling cycle, a total of 23586 bands are observed in the system. The total number of C-C covalent bonds per carbon atom is converged with the criterion of the number of carbon atoms in ideal graphene (1.5 per carbon atom). In this work, the number of covalent bonds is calculated using the distance criterion < 1.6 Å for two carbon atoms.

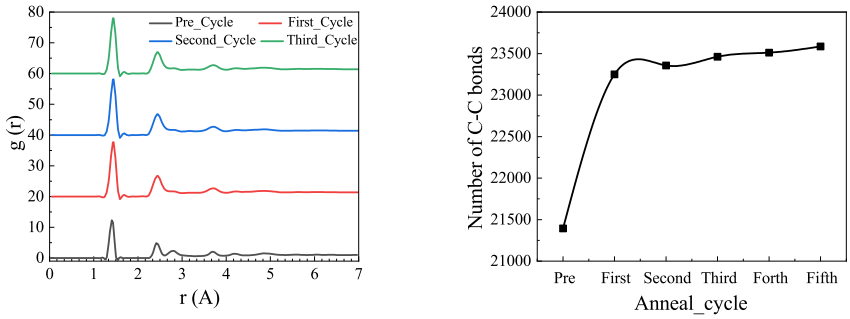

(a) (b)

Figure 6: (a) Radial distribution functions (RDF) related to heating/cooling cycles of the system, (b) The total number of covalent bonds at the end of each heating/cooling cycle of the system.

After the heating and cooling cycles and removing the Au atoms, a stable structure of three-dimensional RGF is obtained. Fig. 7 shows an SEM image of an experimental sample of RGF compared to simulated RGF.

It should be noted that most graphene sheets in walls are adjacent to the junction of several curved joints. Defects cause this curvature in the shape of a pentagon and a hexagon at the grain

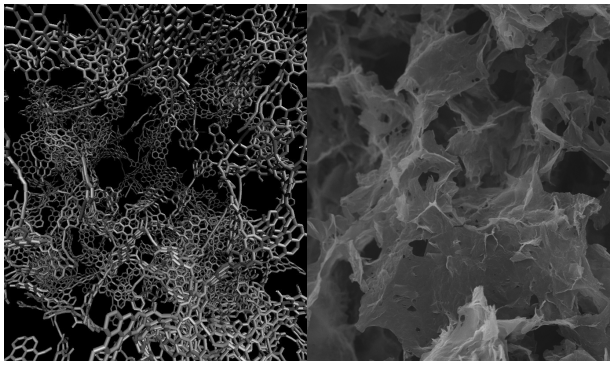

Figure 7: RGF simulated after relaxation stage in dimensions of $100 \times 100 \times 100$ Å^3 compared to the SEM image, Scale bar, 20 μm .

boundary, which cause deformation outside the surface.
In this work, the OVITO package and VMD are used for molecular visualization [20].

4.3. RGF/Epoxy Composite Experimental Tensile Test

In order to evaluate the effect of RGF on the RGF/epoxy composite, tensile tests have been performed. Fig. 8 shows the strain-stress curve for two composite samples reinforced with 100% dried RGF and 95% dried RGF compared to neat epoxy. Adding only 0.63 wt% of graphene in foam to the epoxy and making the RGF/epoxy composite, the Young modulus and tensile strength, the maximum amount of stress in the strain-stress curve, has increased by approximately 169% and 48%, respectively, compared to neat epoxy. This increase indicates a network in the reinforcement and stress transfer from the matrix to the RGF. This three-dimensional network makes the transfer of stress and strain in the whole composite regular and uniform. The synergetic effect of nanoparticles on epoxy is evident, and the Young modulus in the RGF/epoxy composite increases.
The tensile test shows that the tensile strength of RGF/epoxy composite is increased by at least twice that of neat epoxy and graphene/epoxy composites, indicating a three-dimensional bond between the sheets. RGF acts as a barrier to the aggregation of graphene sheets in composites. In addition, a neat epoxy sample for tensile strength was tested to investigate the synergistic effect of RGF reinforced epoxy composites. In the present work, tensile tests were performed for three RGF/epoxy composites. It should be noted that the composite fabrication conditions were the same in all samples, but only the RGF synthesis method was different in the drying step in the laboratory. In the first type of RGF/epoxy composite, RGF is 100% dry, and all viscous motion is minimized; it has the highest resistance to tensile stress compared to the other two types. In the second type, Young modulus and stress strength are weaker than the previous sample in the second type. These foam samples are approximately 95% dry water. The viscoelastic behavior of this type of material after exposure to room temperature causes insufficient mechanical properties compared to 100% dried samples. In the latest type of RGF, after exposure to ambient temperature, cracks appear on the foam surface due to its incomplete drying. Therefore, the sample failed a tensile test at a strain of 2%. The results of the tensile test with reference [15] are compared, that the behavior of composite reinforced with RGF compared to neat epoxy is

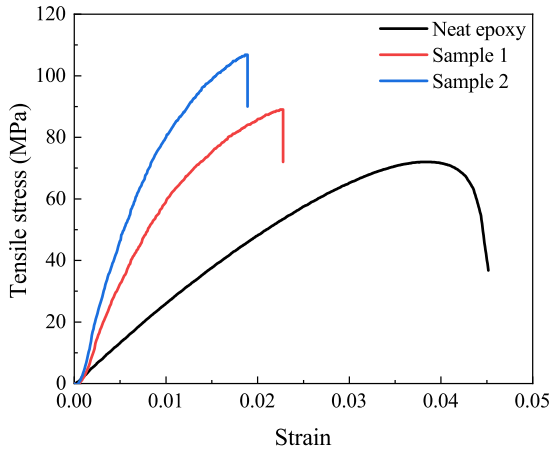

Figure 8: (a) Tensile strain-stress curve of synthesized RGF/epoxy composites under various laboratory conditions and neat epoxy.

correct. It can be noted that the method of synthesis of RGF in this work has better results than the existing samples and can easily control the drying amount of RGF samples.

It should be noted that all samples are fabricated of graphene with the same weight percentage, but different conditions in synthesizing RGF have a significant effect on the amount of elastic modulus and tensile strength. Increasing Young modulus in RGF/epoxy composite samples means they are more brittle and more resistant to axial load than epoxy samples. Also, the increase in tensile strength indicates that composite reinforced with a small weight percentage of graphene sheets in the form of RGF samples can withstand higher loads than neat epoxy samples.

4.4. Tensile Response of Simulated RGF under Uniaxial Loading

To investigate the mechanical properties of RGF under different loading conditions, simulations are performed using LAMMPS MD. The system is first stable under a temperature of 300 K and zero pressure using a Nose-Hoover barostat and the NPT ensemble. At this stage, with a uniform velocity distribution, the system equilibrates at a time of 200 ps and a time step of 0.0001 ps. Fig. 9(a) shows the structure before stretching and the equilibrated system. Using the AIREBO potential and to fully describe the fracture regimes, the cuts-off parameter of the potential was set to 2 Å [35]. By converging the changes in temperature, stress, potential energy, and energy of the whole system with respect to time to a specific value, the system's stability before the employment of the strain rate is guaranteed.

Next, by applying different strain rates, a controlled uniaxial tensile test of deformation was performed in three structure directions. The strain increase was applied to the structure after each time step with a time step of 0.0001 ps. Fig. 10 shows the strain-stress curves of simulated RGF under uniaxial tension in 0.0001, 0.0005, 0.001, and 0.01 ps^{-1} strain rates, respectively. Tensile tests are performed along the x, y, and z axes to ensure computational accuracy and the isotropic behavior of RGF. It is observed that at 300 K, the increase in strain rate has no significant effect on the linear Young modulus. As the strain rate increases, the tensile strength

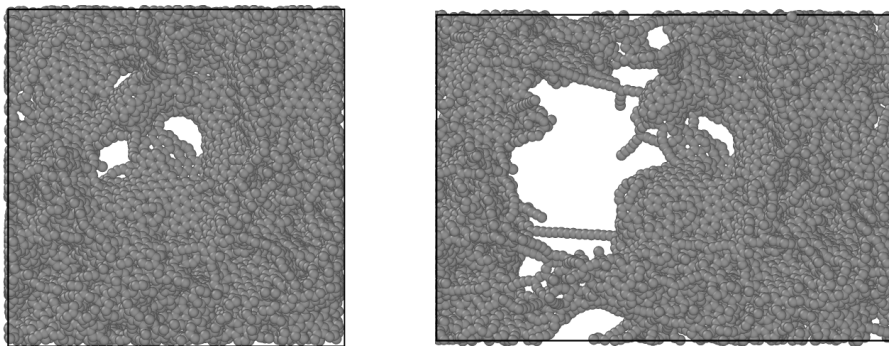

(a) (b)

Figure 9: (a) Molecular dynamics simulation models of structure before tensile test, (b) Simulation snapshot of the full atomic RGF structure in the tensile test.

increase. It should be noted that with decreasing strain rate, computational volume, and time increase, so in this study, the average strain rate of 0.001 ps^{-1} can show the most optimal results. In particular, for each strain rate, two or three independent simulation tests are performed with different initial configurations, and the calculations are repeated several times. Finally, Young modulus and tensile stress for RGF are calculated. The strain parameter in the direction parallel to the deformation is defined as $\varepsilon = L - L_0/L_0$, where L and L_0 are the initial lengths and the simulation box's current lengths in the direction of applying the strain rate. The pressure stress tensor on each atom is calculated to determine the system stress [36]. Finally, the strain-stress diagram is computed to estimate the Young modulus at each strain rate. In addition, Poisson ratio is calculated by defining axial and lateral deformation.

Fig. 9(b) shows a snapshot of the structure during the simulation that after the relaxation step, the system is stretched in the direction of the x-axis with a time step of 0.0001 ps and a strain rate of 0.001 ps^{-1} in the plane strain conditions at a temperature of 300 K.
The Young modulus and tensile strength are equal to the value of about 50 GPa and 5.5 GPa, respectively. The value of Young modulus RGF is compared to the average reported for armchair and zigzag graphene with AIREBO potential in reference [37]. Young modulus and Poisson ratio for the epoxy matrix are used according to the experimental results performed in this work and using the results of molecular dynamics in reference [38].

4.5. CUF-based Micro-Scale Model of the RGF/Epoxy Composite

In this section, the RGF/epoxy composite tensile test analysis is performed using the CUF. The Young modulus and the Poisson ratio of RGF were obtained by the molecular dynamics method. Young modulus and Poisson ratio for the epoxy matrix are used according to the experimental results performed in this work and the results of molecular dynamics in references. The results are shown in Table 1. In this table, E and ν are the Young modulus and Poisson ratio, Ep represents epoxy, and C represents RGF/epoxy composite. This table compares the final Young modulus of RGF, epoxy, and RGF/epoxy composite from the experimental method of this work and the MD method with the multi-scale approach, which has obtained acceptable results. The difference between the numerical model and the experimental model is the existence

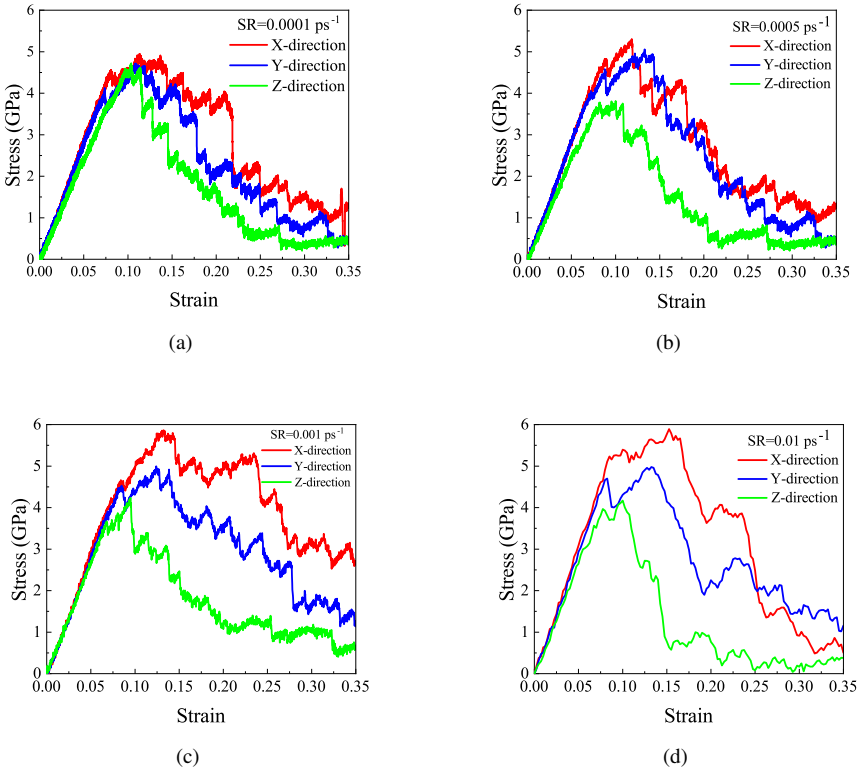

Figure 10: Strain-stress diagram of simulated RGF under tension along the x, y, and z axes strain rate of (a) 0.0001 ps^{-1}, (b) 0.0005 ps^{-1}, (c) 0.001 ps^{-1}, (d) 0.01 ps^{-1}.

of some parameters in laboratory work that are still unknown in numerical methods. Also, some simplifying assumptions in numerical methods can cause differences between numerical results and experiments.

Table 1: Comparison of Young modulus and Poisson ratio of RGF, epoxy and RGF/epoxy composite between experimental and numerical methods

	Method	
Property	Experimental	Numerical
$E_{RGF}\,(GPa)$	–	$50\,(MD)$
v_{RGF}	$-0.3 \leq v \leq 0.46$[39]	$0.33\,(MD)$
$E_{Ep}\,(GPa)$	2.6	$2.6\,(MD)$
v_{Ep}	0.29	$0.29(MD)$
$E_C\,(GPa)$	7.2	$7.3\,(CUF)$

5. CONCLUSIONS

Due to the problem of dispersion graphene sheets in polymer-based composites, three-dimensional graphene foam, RGF, is a way to limit agglomeration in polymers. In the present work, RGF was synthesized using a straightforward and cost-effective HCS method. Then the RGF/epoxy composite was fabricated by the RTM method. After performing validation tests of the foam structure using Raman techniques and SEM images, the composite sample reinforced with RGF was subjected to a tensile test. The tensile test results showed a significant increase in the Young modulus and tensile strength of the RGF/epoxy composite. In RGF with 0.63 wt% by weight filler, Young modulus and tensile strength of RGF/epoxy composites have increased by 169% and 48% compared to neat epoxy, respectively.

In particular, after experimental tests of RGF reinforced polymer composite, using a new multi-step method by molecular dynamics software, simulated the initial structure of RGF using graphene and polycrystalline metal. The simulated RGF was confirmed in density, the number of carbon-carbon bonds, and RDF diagrams with the experimental sample. For the numerical part, the potential of AIREBO, which has high accuracy, has been used, for the subsequent works can also be used of ReaxFF potentials. The RGF simulation added no chemical functional groups to the graphene structure. In particular, simulated RGF was subjected to tensile testing using LAMMPS MD at different strain rates. The numerical simulation results of RGF samples showed that the Young linear modulus did not change significantly with increasing strain rate.

Finally, a high-performance micro-mechanical model based on finite element CUF was used to confirm the experimental analysis. This micromechanical model acts as an efficient tool for calculating the effective stiffness matrix of other properties of periodic heterogeneous composite structures. Demonstrate accurate geometry of components by performing a non-isoparametric mapping technique at no additional cost. CUF-based refined beam theories were also used to model the RGF/epoxy composite RUCs with MSG to obtain suitable governing equations for providing solutions.

As an essential result of this study, it can be found that RGF reinforced composites still do not show significant properties compared to the properties of three-dimensional RGFs. this may be due to some unknown parameters in experimental work or some parameters not considered in numerical work that are very challenging for researchers. Due to the remarkable properties RGFs and polymer composites reinforced with these foams, it is recommended to study the thermal properties of this type of RGF.

References

[1] S. Kumar, R. Purohit, M. Malik, Properties and applications of polymer matrix nano composite materials, Materials Today: Proceedings 2 (4-5) (2015) 3704–3711.

[2] Z. Zheng, X. Zheng, H. Wang, Q. Du, Macroporous graphene oxide–polymer composite prepared through pickering high internal phase emulsions, ACS applied materials & interfaces 5 (16) (2013) 7974–7982.

[3] C. Lee, X. Wei, J. W. Kysar, J. Hone, Measurement of the elastic properties and intrinsic strength of monolayer graphene, science 321 (5887) (2008) 385–388.

[4] A. Vahedi, M. H. S. Lahidjani, S. Shakhesi, Multiscale modeling of thermal conductivity of carbon nanotube epoxy nanocomposites, Physica B: Condensed Matter 550 (2018) 39–46.

[5] L.-C. Tang, Y.-J. Wan, D. Yan, Y.-B. Pei, L. Zhao, Y.-B. Li, L.-B. Wu, J.-X. Jiang, G.-Q. Lai, The effect of graphene dispersion on the mechanical properties of graphene/epoxy composites, Carbon 60 (2013) 16–27.

[6] S. Prolongo, R. Moriche, M. Sánchez, A. Ureña, Self-stratifying and orientation of exfoliated few-layer graphene nanoplatelets in epoxy composites, Composites science and technology 85 (2013) 136–141.

[7] L. Yue, G. Pircheraghi, S. A. Monemian, I. Manas-Zloczower, Epoxy composites with carbon nanotubes and graphene nanoplatelets–dispersion and synergy effects, Carbon 78 (2014) 268–278.

[8] J. Yin, X. Li, J. Zhou, W. Guo, Ultralight three-dimensional boron nitride foam with ultralow permittivity and superelasticity, Nano letters 13 (7) (2013) 3232–3236.
[9] S. Kabiri, D. N. Tran, T. Altalhi, D. Losic, Outstanding adsorption performance of graphene–carbon nanotube aerogels for continuous oil removal, Carbon 80 (2014) 523–533.
[10] J. Wang, X. Gao, Y. Wang, C. Gao, Novel graphene oxide sponge synthesized by freeze-drying process for the removal of 2, 4, 6-trichlorophenol, RSC Advances 4 (101) (2014) 57476–57482.
[11] X. Cao, Y. Shi, W. Shi, G. Lu, X. Huang, Q. Yan, Q. Zhang, H. Zhang, Preparation of novel 3d graphene networks for supercapacitor applications, small 7 (22) (2011) 3163–3168.
[12] K. Olszowska, J. Pang, P. S. Wrobel, L. Zhao, H. Q. Ta, Z. Liu, B. Trzebicka, A. Bachmatiuk, M. H. Rummeli, Three-dimensional nanostructured graphene: synthesis and energy, environmental and biomedical applications, Synthetic Metals 234 (2017) 53–85.
[13] Y. Li, Y. A. Samad, K. Polychronopoulou, S. M. Alhassan, K. Liao, Highly electrically conductive nanocomposites based on polymerinfused graphene sponges, Scientific reports 4 (1) (2014) 1–6.
[14] J. Bong, T. Lim, K. Seo, C.-A. Kwon, J. H. Park, S. K. Kwak, S. Ju, Dynamic graphene filters for selective gas-water-oil separation, Scientific reports 5 (1) (2015) 1–6.
[15] Y. Ni, L. Chen, K. Teng, J. Shi, X. Qian, Z. Xu, X. Tian, C. Hu, M. Ma, Superior mechanical properties of epoxy composites reinforced by 3d interconnected graphene skeleton, ACS applied materials & interfaces 7 (21) (2015) 11583–11591.
[16] Y.-H. Zhao, Y.-F. Zhang, S.-L. Bai, X.-W. Yuan, Carbon fibre/graphene foam/polymer composites with enhanced mechanical and thermal properties, Composites Part B: Engineering 94 (2016) 102–108.
[17] Y.-F. Zhang, Y.-H. Zhao, S.-L. Bai, X. Yuan, Numerical simulation of thermal conductivity of graphene filled polymer composites, Composites Part B: Engineering 106 (2016) 324–331.
[18] Z. Qin, G. S. Jung, M. J. Kang, M. J. Buehler, The mechanics and design of a lightweight three-dimensional graphene assembly, Science advances 3 (1) (2017) e1601536.
[19] A. Pedrielli, S. Taioli, G. Garberoglio, N. M. Pugno, Mechanical and thermal properties of graphene random nanofoams via molecular dynamics simulations, Carbon 132 (2018) 766–775.
[20] F. Rahmani, S. Nouranian, Y. C. Chiew, 3d graphene as an unconventional support material for ionic liquid membranes: Computational insights into gas separations, Industrial & Engineering Chemistry Research 59 (5) (2020) 2203–2210.
[21] A. international, Standard test method for tensile properties of plastics astm d 638-03, Annual book of ASTM standards 8 (2008).
[22] S. Plimpton, Fast parallel algorithms for short-range molecular dynamics, Journal of computational physics 117 (1) (1995) 1–19.
[23] P. Hirel, Atomsk: A tool for manipulating and converting atomic data files, Computer Physics Communications 197 (2015) 212–219.
[24] S. J. Stuart, A. B. Tutein, J. A. Harrison, A reactive potential for hydrocarbons with intermolecular interactions, The Journal of chemical physics 112 (14) (2000) 6472–6486.
[25] J. Kong, Z. Bo, H. Yang, J. Yang, X. Shuai, J. Yan, K. Cen, Temperature dependence of ion diffusion coefficients in nacl electrolyte confined within graphene nanochannels, Physical Chemistry Chemical Physics 19 (11) (2017) 7678–7688.
[26] S. Ding, Y. Tian, Z. Jiang, X. He, Molecular dynamics simulation of joining process of ag-au nanowires and mechanical properties of the hybrid nanojoint, AIP Advances 5 (5) (2015) 057120.
[27] A. G. De Miguel, A. Pagani, W. Yu, E. Carrera, Micromechanics of periodically heterogeneous materials using higher-order beam theories and the mechanics of structure genome, Composite Structures 180 (2017) 484–496.
[28] E. Carrera, A. G. de Miguel, A. Pagani, Micro-, meso-and macro-scale analysis of composite laminates by unified theory of structures, in: ASME International Mechanical Engineering Congress and Exposition, Vol. 58448, American Society of Mechanical Engineers, 2017, p. V009T12A060.
[29] E. Carrera, A. de Miguel, A. Pagani, Component-wise analysis of laminated structures by hierarchical refined models with mapping features and enhanced accuracy at layer to fiber-matrix scales, Mechanics of Advanced Materials and Structures 25 (14) (2018) 1224–1238.
[30] E. Carrera, M. Cinefra, M. Petrolo, E. Zappino, Finite element analysis of structures through unified formulation, John Wiley & Sons, 2014.
[31] W. Yu, A unified theory for constitutive modeling of composites, Journal of Mechanics of Materials and Structures 11 (4) (2016) 379–411.
[32] W. Yu, D. H. Hodges, J. C. Ho, Variational asymptotic beam sectional analysis–an updated version, International Journal of Engineering Science 59 (2012) 40–64.
[33] W. Yu, D. H. Hodges, Asymptotic approach for thermoelastic analysis of laminated composite plates, Journal of Engineering Mechanics 130 (5) (2004) 531–540.
[34] W. Yu, T. Tang, Variational asymptotic method for unit cell homogenization of periodically heterogeneous materi-

als, International Journal of Solids and Structures 44 (11-12) (2007) 3738–3755.
[35] O. Shenderova, D. Brenner, A. Omeltchenko, X. Su, L. Yang, Atomistic modeling of the fracture of polycrystalline diamond, Physical Review B 61 (6) (2000) 3877.
[36] A. P. Thompson, S. J. Plimpton, W. Mattson, General formulation of pressure and stress tensor for arbitrary many-body interaction potentials under periodic boundary conditions, The Journal of chemical physics 131 (15) (2009) 154107.
[37] H. Zhao, K. Min, N. R. Aluru, Size and chirality dependent elastic properties of graphene nanoribbons under uniaxial tension, Nano letters 9 (8) (2009) 3012–3015.
[38] S. Faragi, A. Hamedani, G. Alahyarizadeh, A. Minuchehr, M. Aghaie, B. Arab, Mechanical properties of carbon nanotube-and graphene-reinforced araldite ly/aradur hy 5052 resin epoxy composites: a molecular dynamics study, Journal of molecular modeling 25 (7) (2019) 1–12.
[39] D. Pan, C. Wang, X. Wang, Graphene foam: hole-flake network for uniaxial supercompression and recovery behavior, ACS nano 12 (11) (2018) 11491–11502.